HHS Public Access

Author manuscript

Biomaterials. Author manuscript; available in PMC 2016 October 01.

Published in final edited form as:

Biomaterials. 2015 October ; 67: 183–193. doi:10.1016/j.biomaterials.2015.07.033.

Disulfide cross-linked micelles of novel HDAC inhibitor thailandepsin A for the treatment of breast cancer

Kai Xiao[a,b,1,*], **Yuan-Pei Li**[b,1], **Cheng Wang**[c,§], **Sarah Ahmad**[b], **Michael Vu**[b], **Krishneel Kuma**[b], **Yi-Qiang Cheng**[c], and **Kit S. Lam**[b,**]

[a]National Chengdu Center for Safety Evaluation of Drugs, State Key Laboratory of Biotherapy, Collaborative Innovation Center for Biotherapy, West China Hospital, Sichuan University, Chengdu 610041, P.R. China

[b]Department of Biochemistry & Molecular Medicine, UC Davis Cancer Center, University of California Davis, Sacramento, CA 95817, USA

[c]UNT System College of Pharmacy, University of North Texas Health Science Center, Fort Worth, Texas 76107, USA

Abstract

Histone deacetylase (HDAC) inhibitors are an emerging class of targeted therapy against cancers. Thailandepsin A (TDP-A) is a recently discovered class I HDAC inhibitor with broad anti-proliferative activities. In the present study, we aimed to investigate the potential of TDP-A in the treatment of breast cancer. We demonstrated that TDP-A inhibited cell proliferation and induced apoptosis in breast cancer cells at low nanomolar concentrations. TDP-A activated the intrinsic apoptotic pathway through increase of pro-apoptotic protein Bax, decrease of anti-apoptotic Bcl-2, and cleavage of caspase-3 and poly (ADP-ribose) polymerase (PARP). TDP-A also induced cell cycle arrest at the G2/M phase, and promoted the production of reactive oxygen species (ROS). We have successfully encapsulated TDP-A into our recently developed disulfide cross-linked micelles (DCMs), improving its water solubility and targeted delivery. TDP-A loaded DCMs (TDP-A/DCMs) possess the characteristics of high loading capacity (> 20%, w/w), optimal and monodisperse particle size (16 ± 4 nm), outstanding stability with redox stimuli-responsive disintegration, sustained drug release, and preferential uptake in breast tumors. In the MDA-MB-231 breast cancer xenograft model, TDP-A/DCMs were more efficacious than the FDA-approved FK228 at well-tolerated doses. Furthermore, TDP-A/DCMs exhibited synergistic anticancer effects when combined with the proteasome inhibitor bortezomib (BTZ) loaded DCMs (BTZ/DCMs). Our results indicate that TDP-A nanoformulation alone or in combination with BTZ nanoformulation are efficacious against breast cancer.

[*]Corresponding author. Tel: +86 28 83326313; Fax: +86 28 85173043; iamxiaokai@hotmail.com. [**]Corresponding author. Tel: +1 916 734 0910; Fax: +1 916 734 4418; kit.lam@ucdmc.ucdavis.edu.

[1]These authors contributed equally to this work.

[§]Current address: Cambridge Major Laboratories, Germantown, WI 53022

Keywords

HDAC inhibitor; thailandepsin A; disulfide cross-linked micelle; targeted delivery; breast cancer

1. Introduction

Breast cancer is the most common malignant tumor among women, accounting for an estimated 24% of all cancer cases [1]. Despite significant advances in diagnosis and treatment, breast cancer remains the second leading cause of cancer-related death worldwide; therefore there is a great need for the development of novel therapeutics against this disease. Recently, new treatment strategies focusing on epigenetic intervention have emerged as a promising targeted therapy against cancers, including breast cancer.

Histone deacetylases (HDACs) are a family of enzymes that play an important role in the regulation of gene expression. Abundant evidence shows that aberrant histone acetylation is linked to oncogenesis [2], and overexpression or mutation of HDACs has been often observed in various human cancer tissues, including colon [3], breast [4], prostate [5], lung [6], liver [7], and gastric cancer [8], making HDACs attractive cancer therapeutic targets. Furthermore, inhibition of HDACs has been implicated in cell cycle arrest, cell differentiation and apoptosis. HDAC inhibitors have hence emerged as a new class of anticancer agents. To date, three HDAC inhibitors, synthetic compounds vorinostat (SAHA, Zolinza®) [9], belinostat (PXD-101, Beleodaq®) [10], and natural product FK228 (romidepsin, Istodax®) [11], have been approved by the US Food and Drug Administration (FDA) for the treatment of cutaneous and/or peripheral T-cell lymphomas, and many other HDAC inhibitors, mostly synthetic compounds, are currently being clinically assessed for the treatment of both hematological and solid tumors, often in combination with other anti-cancer drugs.

Thailandepsin A (TDP-A) is a natural and highly potent HDAC inhibitor, recently discovered by means of genome mining from the bacterium *Burkholderia thailandensis* E264 [12]. Similar to FK228, TDP-A has a conserved bicyclic depsipeptide structure (Figure 1A), and its reduced state (with two free thiol groups; not shown) is the active form for HDAC inhibition. TDP-A is able to selectively and strongly inhibit class I HDACs including HDAC1, HDAC2, and HDAC3, with much weaker inhibitory activity toward HDAC4 and HDAC8 than FK228, the latter of which could be beneficial for drug development. TDP-A has shown potent cytotoxic activities against a broad range of cancer cell lines at low to sub-nanomolar concentrations [12–14]. High potency and selective inhibition of class I HDACs qualify TDP-A as a promising epigenetic agent for the treatment of cancers. Here, we aimed to investigate the ability of TDP-A to inhibit breast cancer cell proliferation and tumor growth, and to elucidate the molecular mechanisms underlying these effects.

To overcome the poor water solubility, improve the bioavailability, and increase the tumor accumulation of TDP-A, we have developed a nanoformulation of TDP-A by encapsulating it into our recently invented disulfide cross-linked micelles (DCMs), which is formed by the self-assembly of telodendrimer (PEG^{5k}-Cys_4-L_8-CA_8) [15]. Nanoparticle formulation is

hypothesized to increase the therapeutic index of TDP-A by delivering this experimental drug specifically to tumor sites while sparing normal tissues, *via* the enhanced permeability and retention (EPR) effects [16]. The disulfide bonds in DCMs will prevent the premature release of loaded drugs during circulation, and will be reductively cleaved under the reducing environment of tumor with an elevated glutathione (GSH) concentration after reaching the tumor sites, facilitating the tumor-targeted drug delivery. We previously demonstrated that DCMs were able to deliver the drug more efficiently into tumor sites, resulting in superior antitumor therapeutic efficacy in an ovarian cancer xenograft model, when loaded with chemotherapeutic drug paclitaxel (PTX) [15]. Here, the nanoformulation of TDP-A in DCMs (TDP-A/DCMs) was fully characterized in terms of drug loading efficiency, particle size, stability, drug release profile, *in vitro* cytotoxicity, *in vivo* biodistribution and tumor targeting property.

Bortezomib (BTZ, Velcade®) is a potent proteasome inhibitor approved for the treatment of multiple myeloma and mantle cell lymphoma [17, 18]. Preclinical studies have demonstrated that BTZ exhibits antitumor activity against a broad range of cancers, including breast cancer [19, 20]. Although BTZ as a single agent showed only limited clinical efficacy in a phase II clinical trial [21], when combined with other therapeutics such as doxorubicin [22], capecitabine [23], and docetaxel [24], it delivered promising response rates in patients with metastatic breast cancer. Therefore, in the final part of this study, the *in vivo* anti-cancer effects of TDP-A/DCMs alone or in combination with BTZ/DCMs was investigated in an orthotopic breast cancer xenograft model.

2. Materials and Methods

2.1 Materials

TDP-A (chemical structure, Figure 1A) and FK228 were prepared from bacterial fermentation as reported previously by Cheng group [12, 25]. BTZ was purchased from LC laboratories (Woburn, MA, USA). Annexin V/Propidium Iodide (PI) apoptosis assay kit was purchased from BD Bioscience (San Jose, CA, USA). 1,10-Dioctadecyl-3,3,30,30-tetramethylindodicarbocyanine perchlorate (DiD) and 3,3′-dihexyloxacarbocyanine iodide (DiOC6(3)) were purchased from Life Technologies (Grand Island, NY, USA). PathScan® Intracellular Signaling Array Kit and all antibodies were purchased from Cell Signaling Technology (Danvers, MA, USA). CellTiter 96® AQueous Non-Radioactive Cell Proliferation Assay (MTS) kit was purchased from Promega (Madison, WI, USA). Monomethylterminated poly(ethylene glycol) monoamine (MeO-PEG-NH_2, MW: 5000 Da) was purchased from Rapp Polymere (Tuebingen, Germany). (Fmoc)Lys(Fmoc)-OH was obtained from AnaSpec Inc. (San Jose, CA, USA). 2′,7′-Dichlorofluorescin diacetate (DCF-DA), PD98059, rapamycin, LY294002, Rp-cAMP, sodium dodecyl sulfate (SDS), GSH, PI, RNase, and cholic acid were purchased from Sigma-Aldrich (St. Louis, MO, USA).

2.2 Cell culture and tumor xenograft model

MDA-MB-231 cells were purchased from the American Type Culture Collection (ATCC, Manassas, VA, USA). Cells were cultured in ATCC-formulated Leibovitz's L-15 Medium supplemented with 10% fetal bovine serum, 100 U/mL penicillin G, and 100 mg/mL

streptomycin at 37 °C without CO_2. Human mammary epithelial cells (HuMEC, Invitrogen, Carlsbad, CA, USA) were maintained in HuMEC basal serum-free medium (Invitrogen, #12753018) supplemented with HuMEC supplement kit (Invitrogen, #12755013).

Female athymic nude mice (6–8 weeks old) were purchased from the Harlan Laboratories (Indianapolis, Indiana, USA) and maintained under pathogen-free conditions according to AAALAC guidelines. All animal protocols were approved by the Institutional Animal Care and Use Committee. An orthotopic breast cancer xenograft mouse model was established by injecting 1×10^7 cells in 100 μL of Matrigel/PBS (1:1, v/v) into the fat pad at the base of the nipple.

2.3 Cell viability assay

The *in vitro* cytotoxicity of TDP-A against breast cancer cells was evaluated by MTS assay [26]. Briefly, MDA-MB-231 and HuMEC cells were seeded in 96-well plates, and treated with TDP-A and FK228 ranging from 0.064 nM to 40 nM, respectively. MTS assay was performed to assess cell viability after 72 h of treatment. Cell viability was determined by measuring the percentage of viable cells in the treated group compared to the untreated controls.

2.4 Apoptosis detection, reactive oxygen species (ROS), mitochondrial membrane potential (MMP), and cell cycle analysis

MDA-MB-231 cells were treated with TDP-A for 48 h at concentrations of 1 nM or 4 nM. Cells were stained with Annexin V/PI, and early or late apoptosis was measured by flow cytometric analysis as described previously [27].

The caspase-3/7 activity in the culture medium of MDA-MB-231 cells after 24 h incubation with TDP-A was measured using SensoLyte® Homogeneous AFC Caspase - 3/7 Assay Kit (AnaSpec, Fremont, CA, USA).

MDA-MB-231 cells were incubated with TDP-A for 24 h at concentrations of 1 nM, 2 nM, or 4 nM. Intracellular ROS was measured by flow cytometric analysis using DCF-DA as a fluorescence probe (10 μM). The MMP of MDA-MB-231 cells after 24 h incubation with TDP-A (1, 2, or 4 nM) was measured by flow cytometry using DiOC6(3) (40 nM) staining for 30 min.

For cell cycle analysis, cells were fixed in cold 70% ethanol after 24 h treatment as above. Then, cells were washed with PBS, treated with RNase, and stained with PI (10 μg/ml), followed by flow cytometric analysis.

2.5 Intracellular signaling array and west blot analysis

PathScan® Intracellular Signaling Array Kit was used to simultaneously detect 18 significant and well-characterized signaling molecules when phosphorylated or cleaved, according to the manufacturer's instructions. Briefly, MDA-MB-231 cells were either untreated or treated with TDP-A (2 nM) for 24 h, and the cells were lysed in 1× cell lysis buffer. The lysate was added to each well of assay slides and incubated for 2 h at room temperature. Subsequent to washing, the detection antibody cocktail was added to each well

and incubated for 1 h at room temperature. Horseradish peroxidase (HRP)-linked streptavidin was added to each well and incubated for 30 min at room temperature. The slide was then covered with LumiGLO/Peroxide reagent and exposed for 2–30 sec using a Kodak imaging system IS2000MM.

Several proteins involved in apoptosis and cell cycle regulation were analyzed by western blot. MDA-MB-231 cells were lysed in RIPA buffer (Thermo Fisher Scientific, Waltham, MA, USA) after 24 h or 48 h treatment of TDP-A at different concentrations. Samples were run on sodium dodecyl sulphate-polyacrylamide gels (SDS-PAGEs), transferred onto nitrocellulose membranes, and incubated with appropriate antibodies. Blots were then incubated with HRP-conjugated secondary antibodies and visualized by enhanced chemiluminescence (GE Healthcare, Little Chalfont, Buckinghamshire, UK). The following primary antibodies were used: phosphor-Bad (Ser 112), Bad, caspase 3, BCL-2, Bax, cyclin D1, p21, actin, and α-tubulin.

2.6 Preparation and characterization of TDP-A/DCMs and BTZ/DCMs

PEG^{5k}-Cys_4-L_8-CA_8 telodendrimer was synthesized *via* solution-phase condensation reactions from MeO-PEG-NH_2 utilizing stepwise peptide chemistry as described previously [15]. TDP-A/DCMs and BTZ/DCMs were prepared by the solvent evaporation method as described in previous studies [15, 28]. TDP-A or BTZ was mixed with PEG^{5k}-Cys_4-L_8-CA_8 telodendrimer and dissolved in methanol/chloroform (1:1, v/v). This organic solution was evaporated with a Heidolph rotary evaporator (Elk Grove Village, IL, USA) to form a thin film, followed by hydration of the film with PBS buffer and 30 min of sonication (Cole-Parmer sonicator, Vernon Hills, IL, USA). The resulting drug-loaded micelles were then cross-linked *via* O_2-mediated oxidation as described previously [15]. The drug concentration in TDA-A/DCMs or BTZ/DCMs was analyzed by spectrophotometric detection (262 nm for TDP-A, and 271 nm for BTZ) using a microplate reader (SpectraMax M3, Molecular Devices, Sunnyvale, CA, USA) after releasing the drug from the micelles by adding DMSO (90%, v/v) and 10 min sonication. DCMs mixed with DMSO (1:9, v/v) were used as a blank control. Drug loading was determined using a standard curve generated with a series of TDP-A/DMSO standard solutions (Figure S1 in the Supporting Information). To visualize the cellular uptake and *in vivo* biodistribution of DCMs, the hydrophobic near-infrared (NIRF) dye DiD (0.5 mg/mL) was co-loaded with TDP-A into the disulfide cross-linked micelles using the method described above.

The morphology and particle size distribution of TDP-A/DCMs were characterized by transmission electron microscopy (TEM, Philips CM-120, Amsterdam, Netherland) and dynamic light scattering (DLS) instruments (Microtrac, San Diego, CA, USA), respectively. The drug concentration of TDP-A/DCMs was kept at 1 mg/mL for the duration of the measurement.

The stability of TDP-A/DCMs under physiological and micelle-disrupting conditions was analyzed by monitoring their particle size distribution using DLS. Firstly, TDP-A/DCMs were incubated with 50% (v/v) plasma from healthy human volunteers at physiological body temperature (37 °C) for up to 5 days. Next, TDP-A/DCMs were incubated with SDS (2.5 mg/mL), which was reported to be able to efficiently break down polymeric micelles [29].

Finally, TDP-A/DCMs were incubated with both SDS (2.5 mg/mL) and reducing agent GSH (10 mM). The size distribution of the micelle solutions were measured at predetermined time intervals.

The *in vitro* drug release profile of TDP-A/DCMs was measured using the dialysis method [28]. Aliquots of TDP-A/DCMs (TDP-A loading in DCMs was 1 mg/mL) were injected into dialysis cartridges with a molecular-weight cutoff (MWCO) of 3.5 kDa (Thermo Fisher Scientific, Waltham, MA, USA). Cartridges were dialyzed against 1 L of PBS (or 10 mM GSH) at 37 °C with shaking at 80 rpm (Radnor shaker, VWR, PA, USA) in the presence of activated charcoal (10 g), which created a sink condition. The concentration of TDP-A remaining in the dialysis cartridge at various time points was measured by absorbance spectrophotometry at 262 nm. The release profile of TDP-A (1 mg/mL, in DMSO or cyclodextrin) was determined under the same condition for comparison.

2.7 Cellular uptake, in vitro cytotoxicity, biodistribution, and in vivo histone acetylation inhibition of TDP-A loaded micelles

MDA-MB-231 cells were seeded in 8-well tissue culture chamber slides (BD Biosciences, San Jose, CA) at a density of 50,000 cells per well. After overnight growth, the cells were incubated with DiD-labeled DCMs for 4 h, washed three times with PBS, fixed with 4% paraformaldehyde, and the nuclei stained with DAPI. The slides were mounted with cover slips and observed under confocal laser scanning microscope (Olympus, FV1000, Shinjuku, Tokyo, Japan).

The *in vitro* cytotoxicity of blank DCMs and TDP-A/DCMs against MDA-MB-231 cells was evaluated by MTS assay as described above.

The biodistribution and tumor targeting property of DiD-TDP-A/DCMs were investigated in MDA-MB-231 xenograft mouse model *via* near infrared optical imaging (NIRF) approach. Tumor bearing mice were intravenously injected with DiD-TDP-A/DCMs, and scanned at different time points using a Kodak multimodal imaging system IS2000MM with an excitation at 625 nm and an emission at 700 nm. At 48 h post-injection, tumors and major organs were excised for *ex vivo* imaging.

The *in vivo* inhibition of histone acetylation by TDP-A/DCMs was measured in MDA-MB-231 tumor xenograft after the single dose of 5 mg/kg. At 24 h post-injection, tumor tissue was excised for the immunohistochemistry staining of acetylated H3 expression.

2.8 Cytotoxicity of TDP-A in combination with BTZ

MDA-MB-231 cells were treated with TDP-A (0.4 nM), BTZ (10 nM), or the combination of both. The cell viability and apoptotic activity were measured by MTS assay and caspase 3/7 assay kit, respectively.

2.9 In vivo therapeutic efficacy of TDP-A/DCMs in xenograft model

An orthotopic MDA-MB-231 tumor xenograft model was used to investigate the therapeutic effect of TDP-A/DCMs alone or in combination with BTZ/DCMs. The treatment was initiated when tumor volume reached 100 - 200 mm^3 and this day was designated as day 0.

The maximum tolerated dose (MTD) of FK228 in mice is approximately 2.5 mg/kg [30]. Tumor bearing mice were administered intravenously with PBS control, FK228 (2.5 mg/kg, dissolved in cyclodextrin), TDP-A/DCMs (5 mg/kg), BTZ/DCMs (0.5 mg/kg), or the combination of TDP-A/DCMs (5 mg/kg) with BTZ/DCMs (0.5 mg/kg), respectively. The loading level of TDP-A and BTZ in DCMs were both 1 mg/mL. A total of six doses were given every four days on day 0, 4, 8, 12, 16 and 20. Tumor sizes were measured with a digital caliper twice per week. Tumor volume was calculated by the formula $(L*W^2)/2$, where L is the longest and W is the shortest in tumor diameters (mm). Relative tumor volume (RTV) equals the tumor volume at given time point divided by the tumor volume before initial treatment. The associated toxicities were monitored by body weight measurement twice per week. On the seventh day after the last dose, blood samples were obtained from all mice for measurement of complete blood count (CBC), alanine aminotransferase (ALT), aspartate aminotransferase (AST), total bilirubin, blood urea nitrogen (BUN) and creatinine.

2.10 Statistical analysis

Statistical analysis was performed by Student *t* test for two groups, and one-way ANOVA for multiple groups. All results were expressed as the mean ± standard error (SEM) unless otherwise noted. A value of $P < 0.05$ was considered statistically significant.

3. Results

3.1 TDP-A inhibited HDAC activity and induced cytotoxicity at nanomolar concentrations

The HDAC inhibitory activity of TDP-A was detected in breast cancer cells. MDA-MB-231 cells were treated with different concentrations (0–4 nM) of TDP-A for 24 h, and the levels of acetylated and total histone H3 were measured by western blot. As expected, TDP-A treatment resulted in an increase in acetylation of H3 in MDA-MB-231 cells in a dose-dependent manner (Figure 1B).

The *in vitro* anti-proliferative and cytotoxic activities of TDP-A against breast cancer cells were evaluated by MTS assay. Results showed that TDP-A was notably more potent than FK228 in reducing cell proliferation in MDA-MB-231 cells (Figure 1C), with an IC_{50} of 0.8 nM in comparison of an IC_{50} of 1.4 nM for FK228. To determine the selectivity of TDP-A for cancer cells *vs* normal cells, a cell viability assay was performed on an immortalized human mammary epithelia cell line (HuMEC) that is non-tumorigenic. The cytotoxicity of TDP-A was found to be lower in HuMEC cells than that in MDA-MB-231 cells, with 5.4-fold difference in the IC_{50} values (4.3 nM vs 0.8 nM, Figure S2).

3.2 TDP-A induced apoptosis

The pro-apoptotic activity of TDP-A was examined using two independent assays. First of all, annexin V/PI dual staining was performed in MDA-MB-231 cells after TDP-A treatment for 48 h. Results (Figure 2A) demonstrated that TDP-A treatment led to a significant increase in the populations of cells undergoing early apoptosis (annexin V positive) and late apoptosis (annexin V/PI double positive). Next, the effect of TDP-A on apoptosis was

further confirmed by caspase 3/7 activity assay. As shown in Figure 2B, TDP-A treatment stimulated caspase 3/7 activity in MDA-MB-231 cells in a concentration-dependent manner.

To elucidate the signaling pathways involved in TDP-A induced apoptosis/cytotoxicity, the phosphorylation or cleavage of 18 significant and well-characterized signaling molecules was simultaneously examined using the PathScan Intracellular Signaling array kit. The results (Figure 2C) showed that TDP-A treatment (2 nM) decreased the phosphorylation of p53 at Ser15, increased the cleavage of caspase-3 and PARP, and stimulated the phosphorylation of Bad at Ser-112 site, when compared with the untreated control. In addition, TDP-A treatment also increased the expression of pro-apoptotic protein Bax and reduced the expression of anti-apoptotic protein Bcl-2 in a concentration- and time-dependent manner (Figure 2D). Meanwhile, TDP-A induced caspase-3 cleavage and Bad phosphorylation were validated by western blot analysis (Figure 2E). Several pathways (Ras-MAPK-RSK [31], PI3K-AKT [32], and PKA [33]) were reported to be involved in the regulation of Bad phosphorylation. We further examined whether blockade of these cascades will sensitize breast cancer cells to TDP-A. Specific inhibitors against MAPK (PD98059), ribosome P70S6K (rapamycin), PI3K (LY294002), and PKA (Rp-cAMP) were utilized to block the Bad phosphorylation induced by TDP-A. As expected (Figure S3A), TDP-A-induced Bad phosphorylation at Ser-112 was attenuated by the pretreatment with the inhibitors of MARP, ribosome P70S6K, or PKA, but not with PI3K inhibitor. PI3K-AKT pathway was previously shown to mainly mediate the phosphorylation of Bad at Ser-136 [34]. In addition, MDA-MB-231 cells pretreated with PD98059 or rapamycin and then followed by TDP-A treatment exhibited significantly lower cell viability than those treated with TDP-A alone (Figure S3B), indicating that the inhibition of Bad phosphorylation sensitized breast cancer cells to TDP-A treatment.

3.3 Effect of TDP-A on cell cycle, ROS production, and mitochondrial integrity

The effect of TDP-A on cell cycle progression was evaluated by flow cytometric analysis after 24 h treatment. The results (Figure 3A) demonstrated that TDP-A treatment induced a dose-dependent increase in the percentage of cells in the G2/M phase with a concomitant decrease in G1 phase. In addition, TDP-A treatment (2 nM) also increased the sub G1 population (hypodiploid DNA content), which is a hallmark of apoptosis. Next, western blot analysis was conducted to investigate whether TDP-A altered the expression of genes involved in the cell cycle regulation. As shown in Figure 3B, TDP-A treatment of cells resulted in a dose- and time-dependent decrease in the protein expression of cyclin D1, with no obvious change in p21 expression.

The production of intracellular ROS in cells after exposure to TDP-A was measured by DCF-DA assay. As shown in Figure 3C, TDP-A treatment significantly induced the production of ROS in MDA-MB-231 cells in a concentration-dependent manner.

Loss of mitochondrial membrane potential (MMP) is well known to be an early event during apoptosis. The mitochondrial of MDA-MB-231 cells after TDP-A treatment was stained with DiOC6 dye, and the MMP was measured by flow cytometry. Results demonstrated a concentration-dependent increase in green fluorescence intensity after TDP-A treatment, indicating a loss of MMP in treated cells (Figure 3D).

3.4 Preparation and characterization of TDP-A/DCMs

PEG^{5k}-Cys$_4$-L$_8$-CA$_8$ telodendrimer was synthesized as previously described [15]. Its chemical structure is illustrated in Figure S4, which consists of a dendritic oligomer of cholic acids attached to one terminus of the linear PEG through a poly(lysine-cysteine-Ebes) backbone. The molecular weight of PEG^{5k}-Cys$_4$-L$_8$-CA$_8$ telodendrimer was 11,198 daltons obtained *via* MALDI-TOF mass spectrometry analysis. The self-assembly of PEG^{5k}-Cys$_4$-L$_8$-CA$_8$ telodendrimer followed by oxidation was able to form DCMs, with the critical micelle concentration (CMC) of 0.67 μM, and the near neutral zeta potential [15]. The hydrophobic HDAC inhibitor TDP-A can be easily encapsulated into DCMs. The loading efficiency (LE) of TDP-A into DCMs was almost 100% when the initial amount of TDP-A was ≤ 10% (w/w) of PEG^{5k}-Cys$_4$-L$_8$-CA$_8$ telodendrimer, and decreased gradually when the initial amount increased (Figure 4A). TDP-A/DCMs retained a similar particle size distribution ranging from 15 to 20 nm, when the drug loading level was lower than 4 mg/mL TDP-A in 20 mg/mL telodendrimer. The particle size distribution and morphology of TDP-A/DCMs were measured by DLS and TEM, respectively. As determined by DLS (Figure 4B), TDP-A/DCMs (TDP-A loading level was 1 mg/mL) displayed a narrow particle size distribution with a polydispersity index (PDI) of 0.18, and the average size was 16 ± 4 nm in diameter. The morphology of TDP-A/DCMs was observed to be spherical under TEM (Figure 4C), and the size was consistent with that measured by DLS.

The stability of TDP-A/DCMs in physiological and severe micelle disrupting conditions was investigated. TDP-A/DCMs were incubated with 50% human plasma at 37 °C, and their size was monitored over time using DLS. As shown in Figure S5A, the particle size of TDP-A/DCMs was very stable during the 110 h period. The stability of TDP-A/DCMs was also examined in the presence of SDS (2.5 mg/mL), a surfactant known to disrupt polymeric micelles [29]. The particle size of TDP-A/DCMs remained unchanged during the addition of SDS, indicating that the micelles remain intact. However, upon the addition of reducing agent such as GSH (10 mM), the integrity of TDP-A/DCMs was compromised and complete disruption of micelles was observed after 30 min (Figure S5B). Since the intracellular concentration of GSH is substantially higher than the extracellular level (10 mM vs 2 μM) [35], the redox stimuli-responsive disintegration of DCMs will facilitate the rapid drug release inside cancer cells once TDP-A/DCMs has accumulated at the tumor sites.

The drug release profile of TDP-A/DCMs was measured by the dialysis method, when compared with that of TDP-A in DMSO, or in cyclodextrin (Figure 4D). About 86% or 50% of TDP-A was released from DMSO or cyclodextrin, respectively, within the first 4 h. By 24 h, almost 100% of TDP-A in DMSO or cyclodextrin had been released, whereas only 26% of TDP-A was released from TDP-A/DCMs and the slow drug release was sustained for more than one week. Furthermore, as predicted, the release rate of TDP-A/DCMs was significantly accelerated in the presence of reducing agent GSH (10 mM).

3.5 In vitro cellular uptake, cytotoxicity, and in vivo biodistribution of TDP-A/DCMs

The cellular uptake of TDP-A/DCMs with fluorescent labeling was observed in MDA-MB-231 cells after 4 h incubation. Confocal microscopy images demonstrated that TDP-A/

DCMs were able to be internalized into cells, and mainly distributed in the cytoplasmic region upon their uptake (Figure 5A).

The *in vitro* cytotoxicity of free TDP-A, blank DCMs and TDP-A/DCMs was evaluated in MDA-MB-231 cells by MTS assay. As shown in Figure 5B, blank DCMs did not show detectable cytotoxicity at the tested concentrations, while TDP-A/DCMs exhibited comparable cytotoxic activity with free TDP-A, with the IC_{50} of approximately 1 nM.

To effectively track nanoparticles *in vivo*, TDP-A/DCMs were fluorescently labeling with the NIRF dye DiD, which is known to enhance deep tissue imaging by high penetration in addition to low tissue absorption and scattering. The *in vivo* biodistribution and tumor accumulation of DiD-TDP-A/DCMs were investigated in orthotopic MDA-MB-231 xenograft bearing mice *via* NIRF optical imaging approach. DiD-TDP-A/DCMs were found to gradually accumulate into tumor site starting 1 h after systematic administration, and high contrast of fluorescence signal between tumor and normal tissue sustained up to at least 48 h (Figure 5C). *Ex vivo* imaging at 48 h post-injection further confirmed the preferential uptake of DCMs in tumor compared to normal organs except the liver (Figure 5D).

3.6 Synergistic cytotoxicity of TDP-A in combination with bortezomib (BTZ)

Proteasome inhibitor BTZ showed concentration-dependent cytotoxicity against MDA-MB-231 cells following 72 h exposure, with an IC_{50} of 10 nM (Figure S6A). Treatment of cells with the combination of TDP-A (0.4 nM) and BTZ (10 nM) led to significant increase in apoptosis (Figure 6A) and induction of cell death (Figure 6B), indicating their synergistic effect against breast cancer cells.

3.7 In vivo HDAC inhibition, therapeutic efficacy, and toxicity of TDP-A/DCMs in breast cancer xenograft models

The *in vivo* HDAC inhibitory activity of TDP-A/DCMs was evaluated in the xenograft model of breast cancer. MDA-MB-231 tumor-bearing mice were administered intravenously with TDP-A/DCMs at the dose of 5 mg/kg, and the histone acetylation level in tumor tissue at 24 h post-injection was assessed by immunohistochemistry. As shown in Figure 7A, TDP-A nanoformulation substantially increased the acetylated histone H3 level of tumor tissue when compared to PBS control.

The *in vivo* antitumor efficacy of TDP-A/DCMs alone or in combination with BTZ/DCMs was investigated in an orthotopic xenograft model of breast cancer. BTZ/DCMs had the particle size of around 16 nm with narrow distribution (Figure S6B), and exhibited excellent stability in human plasma for a few days (Figure S6C, D). The single-dose MTD of TDP-A in mice was 12.5 mg/kg, based on the preliminary data generated by NCI-Developmental Therapeutics Program (DTP) (unpublished), and the micellar formulations were expected to be better tolerated than free drug according to our previous report [28, 36]. Given the repeated dose and the combination with BTZ in the therapeutic study, a lower dose (5 mg/kg) than MTD was chosen for TDP-A/DCMs. MDA-MB-231 tumor bearing mice were administered intravenously with PBS control, free FK228 (2.5 mg/kg, MTD), TDP-A/DCMs (5 mg/kg), BTZ/DCMs (0.5 mg/kg), and combined TDP-A/DCMs (5 mg/kg) with BTZ/

DCMs (0.5 mg/kg), respectively. A total of six doses were given every four days on day 0, 4, 8, 12, 16 and 20. As shown in Figure 7B, all the treatment caused a significant inhibition in tumor growth as compared to the PBS control ($P < 0.05$). At nearly equitoxic dose of FK228 (comparable body weight loss), TDP-A/DCMs demonstrated superior tumor growth inhibition ($P < 0.05$). Furthermore, the combination of TDP-A/DCMs and BTZ/DCMs exerted strong synergy in tumor growth inhibition, when compared to each treatment alone ($P < 0.05$).

Potential toxicities associated with treatment were monitored by body weight change, CBC, and serum chemistry (hepatic and renal function panel test). Although mice treated with free FK228, TDP-A/DCMs, or the combination of TDP-A/DCMs and BTZ/DCMs showed transient slight body weight loss (less than 6.5%) during the treatment cycle, a rapid increase in weight was observed in mice after the end of treatment. CBC results on day 7 of the last dosage showed that WBC, RBC, hemoglobin and platelet in all the groups were within the normal range and excluded the potential hematologic toxicity (Table S1). Serum chemistry (ALT, AST, total bilirubin, BUN and creatinine) in all the groups was also within the normal range (Table S2), indicating an absence of hepatic and renal toxicity.

4. Discussion

HDAC inhibitors represent a promising targeted therapy for resistant and aggressive malignancies. TDP-A is a recently reported HDAC inhibitor with improved potency and class I HDACs selectivity, and exhibits potent cytotoxic activity in different cancer cells [12–14]. Class I HDACs (HDAC1, HDAC2 and HDAC3) are frequently overexpressed in human tumors including breast cancer [4, 37], and knockdown of HDAC1 or HDAC2 is sufficient to reduce tumor growth *in vivo* [38]. In the present study, we examined the feasibility of using TDP-A alone or in combination with other anticancer agents for the treatment of breast cancer.

We have shown that TDP-A inhibits HDAC activity and up-regulates the expression of acetylated histone H3 in both human breast cancer cell lines and tumor xenograft models. TDP-A exhibited selective and potent cytotoxic effects against breast cancer cells compared with normal cells. The mechanisms underlying TDP-A-mediated cell death were further explored, and our data suggested that multiple mechanisms were potentially involved. Firstly, TDP-A treatment induced apoptosis in breast cancer cells. It was reported that HDAC inhibitors could induce apoptosis *via* either intrinsic (mitochondrial) or extrinsic (death receptor) pathway [39]. Our data demonstrated that TDP-A activated the intrinsic pathway through up-regulation of pro-apoptotic proteins such as Bax, and down-regulation of anti-apoptotic proteins such as Bcl-2. The activation resulted in increased MMP, which will promote the release of mitochondrial membrane proteins, such as cytochrome C, AIF and Smac, and ultimately activate caspase-3. Increased levels of cleaved caspase-3 and cleaved PARP are reliable indicators of apoptosis. Interestingly, treatment of cells with TDP-A also stimulated the phosphorylation of Bad at Ser-112 *via* the ERK or/and PKA cascades, indicating TDP-A inhibited the pro-apoptotic effect of Bad. Inhibition of Bad phosphorylation of Bad by ERK/PKA inhibitors potentiated the cytotoxic effects of TDP-A against breast cancer cells. These findings suggest the potential clinical use of ERK or PKA

inhibitors to improve the therapeutic response of TDP-A. Secondly, TDP-A induced cell cycle arrest at G2/M phase in breast cancer cells. Western blot analysis demonstrated that the level of p21 protein was unchanged, but cyclin D1 was down-regulated in MDA-MB-231 cells following TDP-A treatment. Cyclin D1 is an important regulator of cell cycle progression, and it is down-regulated in response to oxidative stress and implicated in the induction of cell cycle arrest in G2 phase by an unknown mechanism [40]. Thirdly, TDP-A induced the generation of ROS in breast cancer cells. A number of studies have reported that HDAC inhibitors, such as vorinostat [41] and trichostatin A (TSA) [42], are able to induce ROS production in different malignant cell types. Accumulation of ROS may cause DNA damage, oxidative stress, and subsequent apoptosis.

Polymeric micelles have been extensively investigated for the delivery of anticancer drugs, and provide several distinct advantages, including improved solubility, prolonged *in vivo* circulation time and preferential accumulation at tumor site *via* the EPR effect. Stimuli-responsive cross-linked micelles are able to minimize the premature drug release during blood circulation, and release the drug upon stimuli present in the tumor microenvironment [43]. We have recently developed a novel class of DCMs based on the self-assembly of thiolated PEG-oligocholic acid telodendrimer, which was successfully applied for the delivery of paclitaxel [15], vincristine [44]. In the present study, we have shown that TDP-A can be readily incorporated into DCMs with high loading capacity, uniform and optimal particle size. TDP-A/DCMs exhibited outstanding stability in physiological condition (human plasma) and even in severe micelle disrupting condition such as SDS, and disintegrated in the addition of a reducing agent GSH at the physiological concentration in cancer cells. The superior stability in blood and redox stimuli-responsive characteristics of TDP-A/DCMs will be expected to prevent the premature drug release and deliver drugs more efficiently into tumor tissue and cells. TDP-A/DCMs showed a sustained release of TDP-A from the nanocarrier over time, which is desirable for the in *vivo* applications. TDP-A/DCMs were able to be internalized into breast cancer cells and exhibited similar cytotoxic effects as free TDP-A. Biodistribution study demonstrated that DiD-TDP-A/DCMs preferentially accumulated into the tumor sites, which is likely due to the passive targeting of nano-sized DCMs *via* the prolonged circulation and EPR effect. Upon the uptake into cancer cells, the intracellular reducing environment (high GSH level) will reduce the disulfide bonds of DCMs, facilitate the fast release of TDP-A, and also reduce TDP-A to its activated form. In the therapeutic study, the antitumor efficacy of TDP-A/DCMs in breast cancer xenograft models was superior to free FK228 at the well-tolerated dose, which can be attributed to the high potency of TDP-A, and nanoparticle-mediated efficient drug delivery into tumor sites. Although some uptake of DCMs in the liver was observed through NIRF imaging due to the nonspecific clearance by Kupffer cells [45], there was no sign of hepatotoxicity in mice treated with the TDP-A/DCMs, as confirmed by serum chemistry analysis. Besides, no other observable side effects were noted in the treated mice, suggesting the TDP-A nanoformulation exhibits cancer cells targeting with low “off-target” toxicity.

HDAC inhibitors have shown synergistic or additive antitumor effects with other chemotherapeutic drugs, targeted therapeutic reagents and radiation, by various mechanisms. BTZ as a proteasome inhibitor showed limited clinical response in metastatic

breast cancers, but achieved promising therapeutic effects when combined with other anticancer agents [46]. In this study, our data demonstrated that TDP-A can sensitize breast cancer cells to BTZ treatment, as evidenced by significantly increased apoptosis and cytotoxicity in the *in vitro* study. Furthermore, we were able to encapsulate BTZ into our DCMs, and demonstrated that the combination with BTZ/DCMs further improved the therapeutic outcome of TDP-A/DCMs in breast cancer xenograft models. The specific mechanisms responsible for the synergic effect remain unclear, and warrant further study. It was also reported that combined BTZ with HDAC inhibitors (PXD101 and PCI024781) exhibited synergistic apoptosis in multiple myeloma and lymphoma cell line [47, 48]. It is proposed that the synergistic interactions between BTZ and HDAC inhibitors involve multiple mechanisms, including enhanced generation of ROS and oxidative stress, proteasome and NF-κB inhibition.

5. Conclusion

We have demonstrated that TDP-A has potent HDAC inhibition and anti-proliferative activity in breast cancer cells. Multiple molecular mechanisms were involved in the cytotoxicity of TDP-A, including the induction of apoptosis *via* the intrinsic pathway, G2/M cell cycle arrest, and generation of ROS. TDP-A can be easily formulated into our previously developed DCMs, and the TDP-A/DCMs formulation has high loading capacity, optimal particle size, outstanding stability, sensitive redox-response, and sustained drug release profiles. TDP-A/DCMs with NIRF fluorescent labeling showed preferential uptake in the breast tumor xenograft based on their prolonged blood circulation and EPR effect. TDP-A/DCMs exhibited superior anti-tumor efficacy with low toxicity in breast cancer xenograft models, when compared to FDA-approved FK228. Furthermore, the combination of TDP-A/DCMs with proteasome inhibitor BTZ/DCMs resulted in synergistic anti-tumor activity. Taken together, our data suggest that TDP-A nanoformulation has promising therapeutic potential in breast cancer, either as a single agent or in combination with BTZ nanoformulation.

Supplementary Material

Refer to Web version on PubMed Central for supplementary material.

Acknowledgments

The authors acknowledge the editorial assistance from Dr. Randy Carney, and the financial support from NIH/NCI R01CA152212 (to Y.-Q.C.), R01CA115483 and R01EB012569 (to K.S.L.), DOD BCRP Postdoctoral Award (W81XWH-10-1-0817, to K.X.), and National Natural Sciences Foundation of China (81101143, to K.X.)

Reference

1. Jemal A, Center MM, DeSantis C, Ward EM. Global patterns of cancer incidence and mortality rates and trends. Cancer Epidemiol Biomarkers Prev. 2010 Aug; 19(8):1893–1907. [PubMed: 20647400]
2. Ozdag H, Teschendorff AE, Ahmed AA, Hyland SJ, Blenkiron C, Bobrow L, et al. Differential expression of selected histone modifier genes in human solid cancers. BMC Genomics. 2006; 7:90. [PubMed: 16638127]

3. Weichert W, Roske A, Niesporek S, Noske A, Buckendahl AC, Dietel M, et al. Class I histone deacetylase expression has independent prognostic impact in human colorectal cancer: specific role of class I histone deacetylases in vitro and in vivo. Clin Cancer Res. 2008 Mar 15; 14(6):1669–1677. [PubMed: 18347167]
4. Krusche CA, Wulfing P, Kersting C, Vloet A, Bocker W, Kiesel L, et al. Histone deacetylase-1 and-3 protein expression in human breast cancer: a tissue microarray analysis. Breast Cancer Res Treat. 2005 Mar; 90(1):15–23. [PubMed: 15770522]
5. Weichert W, Roske A, Gekeler V, Beckers T, Stephan C, Jung K, et al. Histone deacetylases 1, 2 and 3 are highly expressed in prostate cancer and HDAC2 expression is associated with shorter PSA relapse time after radical prostatectomy. Br J Cancer. 2008 Feb 12; 98(3):604–610. [PubMed: 18212746]
6. Minamiya Y, Ono T, Saito H, Takahashi N, Ito M, Mitsui M, et al. Expression of histone deacetylase 1 correlates with a poor prognosis in patients with adenocarcinoma of the lung. Lung Cancer. 2011 Nov; 74(2):300–304. [PubMed: 21466904]
7. Rikimaru T, Taketomi A, Yamashita Y, Shirabe K, Hamatsu T, Shimada M, et al. Clinical significance of histone deacetylase 1 expression in patients with hepatocellular carcinoma. Oncology. 2007; 72(1–2):69–74. [PubMed: 18004079]
8. Weichert W, Roske A, Gekeler V, Beckers T, Ebert MP, Pross M, et al. Association of patterns of class I histone deacetylase expression with patient prognosis in gastric cancer: a retrospective analysis. Lancet Oncol. 2008 Feb; 9(2):139–148. [PubMed: 18207460]
9. Duvic M, Talpur R, Ni X, Zhang C, Hazarika P, Kelly C, et al. Phase 2 trial of oral vorinostat (suberoylanilide hydroxamic acid, SAHA) for refractory cutaneous T-cell lymphoma (CTCL). Blood. 2007 Jan 1; 109(1):31–39. [PubMed: 16960145]
10. Lee HZ, Kwitkowski VE, Del Valle PL, Ricci MS, Saber H, Habtemariam BA, et al. FDA Approval: Belinostat for the Treatment of Patients with Relapsed or Refractory Peripheral T-cell Lymphoma. Clinical cancer research : an official journal of the American Association for Cancer Research. 2015 Jun 15; 21(12):2666–2670. [PubMed: 25802282]
11. VanderMolen KM, McCulloch W, Pearce CJ, Oberlies NH. Romidepsin (Istodax, NSC 630176, FR901228, FK228, depsipeptide): a natural product recently approved for cutaneous T-cell lymphoma. The Journal of antibiotics. 2011 Aug; 64(8):525–531. [PubMed: 21587264]
12. Wang C, Henkes LM, Doughty LB, He M, Wang D, Meyer-Almes FJ, et al. Thailandepsins: bacterial products with potent histone deacetylase inhibitory activities and broad-spectrum antiproliferative activities. Journal of natural products. 2011 Oct 28; 74(10):2031–2038. [PubMed: 21793558]
13. Wilson AJ, Cheng YQ, Khabele D. Thailandepsins are new small molecule class I HDAC inhibitors with potent cytotoxic activity in ovarian cancer cells: a preclinical study of epigenetic ovarian cancer therapy. Journal of ovarian research. 2012; 5(1):12. [PubMed: 22531354]
14. Weinlander E, Somnay Y, Harrison AD, Wang C, Cheng YQ, Jaskula-Sztul R, et al. The novel histone deacetylase inhibitor thailandepsin A inhibits anaplastic thyroid cancer growth. The Journal of surgical research. 2014 Jul; 190(1):191–197. [PubMed: 24679699]
15. Li Y, Xiao K, Luo J, Xiao W, Lee JS, Gonik AM, et al. Well-defined, reversible disulfide cross-linked micelles for on-demand paclitaxel delivery. Biomaterials. 2011 Sep; 32(27):6633–6645. [PubMed: 21658763]
16. Matsumura Y, Maeda H. A new concept for macromolecular therapeutics in cancer chemotherapy: mechanism of tumoritropic accumulation of proteins and the antitumor agent smancs. Cancer Res. 1986 Dec; 46(12 Pt 1):6387–6392. [PubMed: 2946403]
17. Orlowski RZ, Kuhn DJ. Proteasome inhibitors in cancer therapy: lessons from the first decade. Clin Cancer Res. 2008 Mar 15; 14(6):1649–1657. [PubMed: 18347166]
18. Voorhees PM, Orlowski RZ. The proteasome and proteasome inhibitors in cancer therapy. Annu Rev Pharmacol Toxicol. 2006; 46:189–213. [PubMed: 16402903]
19. Cardoso F, Ross JS, Picart MJ, Sotiriou C, Durbecq V. Targeting the ubiquitin-proteasome pathway in breast cancer. Clin Breast Cancer. 2004 Jun; 5(2):148–157. [PubMed: 15245620]

20. Codony-Servat J, Tapia MA, Bosch M, Oliva C, Domingo-Domenech J, Mellado B, et al. Differential cellular and molecular effects of bortezomib, a proteasome inhibitor, in human breast cancer cells. Mol Cancer Ther. 2006 Mar; 5(3):665–675. [PubMed: 16546981]
21. Yang CH, Gonzalez-Angulo AM, Reuben JM, Booser DJ, Pusztai L, Krishnamurthy S, et al. Bortezomib (VELCADE) in metastatic breast cancer: pharmacodynamics, biological effects, and prediction of clinical benefits. Ann Oncol. 2006 May; 17(5):813–817. [PubMed: 16403809]
22. Irvin WJ Jr, Orlowski RZ, Chiu WK, Carey LA, Collichio FA, Bernard PS, et al. Phase II study of bortezomib and pegylated liposomal doxorubicin in the treatment of metastatic breast cancer. Clin Breast Cancer. 2010 Dec 1; 10(6):465–470. [PubMed: 21147690]
23. Schmid P, Kuhnhardt D, Kiewe P, Lehenbauer-Dehm S, Schippinger W, Greil R, et al. A phase I/II study of bortezomib and capecitabine in patients with metastatic breast cancer previously treated with taxanes and/or anthracyclines. Ann Oncol. 2008 May; 19(5):871–876. [PubMed: 18209010]
24. Awada A, Albanell J, Canney PA, Dirix LY, Gil T, Cardoso F, et al. Bortezomib/docetaxel combination therapy in patients with anthracycline-pretreated advanced/metastatic breast cancer: a phase I/II dose-escalation study. Br J Cancer. 2008 May 6; 98(9):1500–1507. [PubMed: 18454159]
25. Wesener SR, Potharla VY, Cheng YQ. Reconstitution of the FK228 biosynthetic pathway reveals cross talk between modular polyketide synthases and fatty acid synthase. Applied and environmental microbiology. 2011 Feb; 77(4):1501–1507. [PubMed: 21183648]
26. Xiao K, Luo J, Li Y, Lee JS, Fung G, Lam KS. PEG-oligocholic acid telodendrimer micelles for the targeted delivery of doxorubicin to B-cell lymphoma. J Control Release. 2011 Oct 30; 155(2): 272–281. [PubMed: 21787818]
27. Dasmahapatra G, Lembersky D, Kramer L, Fisher RI, Friedberg J, Dent P, et al. The pan-HDAC inhibitor vorinostat potentiates the activity of the proteasome inhibitor carfilzomib in human DLBCL cells in vitro and in vivo. Blood. 2010 Jun 3; 115(22):4478–4487. [PubMed: 20233973]
28. Xiao K, Luo J, Fowler WL, Li Y, Lee JS, Xing L, et al. A self-assembling nanoparticle for paclitaxel delivery in ovarian cancer. Biomaterials. 2009 Oct; 30(30):6006–6016. [PubMed: 19660809]
29. Koo AN, Lee HJ, Kim SE, Chang JH, Park C, Kim C, et al. Disulfide-cross-linked PEG-poly(amino acid)s copolymer micelles for glutathione-mediated intracellular drug delivery. Chem Commun (Camb). 2008 Dec; 28(48):6570–6572. [PubMed: 19057782]
30. Nishida K, Komiyama T, Miyazawa S, Shen ZN, Furumatsu T, Doi H, et al. Histone deacetylase inhibitor suppression of autoantibody-mediated arthritis in mice via regulation of p16INK4a and p21(WAF1/Cip1) expression. Arthritis Rheum. 2004 Oct; 50(10):3365–3376. [PubMed: 15476220]
31. Fang X, Yu S, Eder A, Mao M, Bast RC Jr, Boyd D, et al. Regulation of BAD phosphorylation at serine 112 by the Ras-mitogen-activated protein kinase pathway. Oncogene. 1999 Nov 18; 18(48): 6635–6640. [PubMed: 10597268]
32. Datta SR, Dudek H, Tao X, Masters S, Fu H, Gotoh Y, et al. Akt phosphorylation of BAD couples survival signals to the cell-intrinsic death machinery. Cell. 1997 Oct 17; 91(2):231–241. [PubMed: 9346240]
33. Harada H, Becknell B, Wilm M, Mann M, Huang LJ, Taylor SS, et al. Phosphorylation and inactivation of BAD by mitochondria-anchored protein kinase A. Mol Cell. 1999 Apr; 3(4):413–422. [PubMed: 10230394]
34. del Peso L, Gonzalez-Garcia M, Page C, Herrera R, Nunez G. Interleukin-3-induced phosphorylation of BAD through the protein kinase Akt. Science. 1997 Oct 24; 278(5338):687–689. [PubMed: 9381178]
35. Li YL, Zhu L, Liu Z, Cheng R, Meng F, Cui JH, et al. Reversibly stabilized multifunctional dextran nanoparticles efficiently deliver doxorubicin into the nuclei of cancer cells. Angew Chem Int Ed Engl. 2009; 48(52):9914–9918. [PubMed: 19937876]
36. Xiao K, Li Y, Lee JS, Gonik AM, Dong T, Fung G, et al. "OA02" peptide facilitates the precise targeting of paclitaxel-loaded micellar nanoparticles to ovarian cancer in vivo. Cancer research. 2012 Apr 15; 72(8):2100–2110. [PubMed: 22396491]

37. Zhang Z, Yamashita H, Toyama T, Sugiura H, Ando Y, Mita K, et al. Quantitation of HDAC1 mRNA expression in invasive carcinoma of the breast*. Breast Cancer Res Treat. 2005 Nov; 94(1):11–16. [PubMed: 16172792]

38. Haberland M, Johnson A, Mokalled MH, Montgomery RL, Olson EN. Genetic dissection of histone deacetylase requirement in tumor cells. Proc Natl Acad Sci U S A. 2009 May 12; 106(19): 7751–7755. [PubMed: 19416910]

39. Dickinson M, Johnstone RW, Prince HM. Histone deacetylase inhibitors: potential targets responsible for their anti-cancer effect. Invest New Drugs. 2010 Dec; 28(Suppl 1):S3–S20. [PubMed: 21161327]

40. Pyo CW, Choi JH, Oh SM, Choi SY. Oxidative stress-induced cyclin D1 depletion and its role in cell cycle processing. Biochim Biophys Acta. 2013 Nov; 1830(11):5316–5325. [PubMed: 23920145]

41. Petruccelli LA, Dupere-Richer D, Pettersson F, Retrouvey H, Skoulikas S, Miller WH Jr. Vorinostat induces reactive oxygen species and DNA damage in acute myeloid leukemia cells. PLoS One. 2011; 6(6):e20987. [PubMed: 21695163]

42. Liu F, Yu G, Wang G, Liu H, Wu X, Wang Q, et al. An NQO1-initiated and p53-independent apoptotic pathway determines the anti-tumor effect of tanshinone IIA against non-small cell lung cancer. PLoS One. 2012; 7(7):e42138. [PubMed: 22848731]

43. Li Y, Xiao K, Zhu W, Deng W, Lam KS. Stimuli-responsive cross-linked micelles for on-demand drug delivery against cancers. Adv Drug Deliv Rev. 2013 Feb; 66(2013):58–73. [PubMed: 24060922]

44. Kato J, Li Y, Xiao K, Lee JS, Luo J, Tuscano JM, et al. Disulfide cross-linked micelles for the targeted delivery of vincristine to B-cell lymphoma. Molecular pharmaceutics. 2012 Jun 4; 9(6): 1727–1735. [PubMed: 22530955]

45. Xiao K, Li Y, Luo J, Lee JS, Xiao W, Gonik AM, et al. The effect of surface charge on in vivo biodistribution of PEG-oligocholic acid based micellar nanoparticles. Biomaterials. 2011 May; 32(13):3435–3446. [PubMed: 21295849]

46. Tseng LM, Liu CY, Chang KC, Chu PY, Shiau CW, Chen KF. CIP2A is a target of bortezomib in human triple negative breast cancer cells. Breast Cancer Res. 2012; 14(2):R68. [PubMed: 22537901]

47. Feng R, Oton A, Mapara MY, Anderson G, Belani C, Lentzsch S. The histone deacetylase inhibitor, PXD101, potentiates bortezomib-induced anti-multiple myeloma effect by induction of oxidative stress and DNA damage. Br J Haematol. 2007 Nov; 139(3):385–397. [PubMed: 17910628]

48. Bhalla S, Balasubramanian S, David K, Sirisawad M, Buggy J, Mauro L, et al. PCI-24781 induces caspase and reactive oxygen species-dependent apoptosis through NF-kappaB mechanisms and is synergistic with bortezomib in lymphoma cells. Clin Cancer Res. 2009 May 15; 15(10):3354–3365. [PubMed: 19417023]

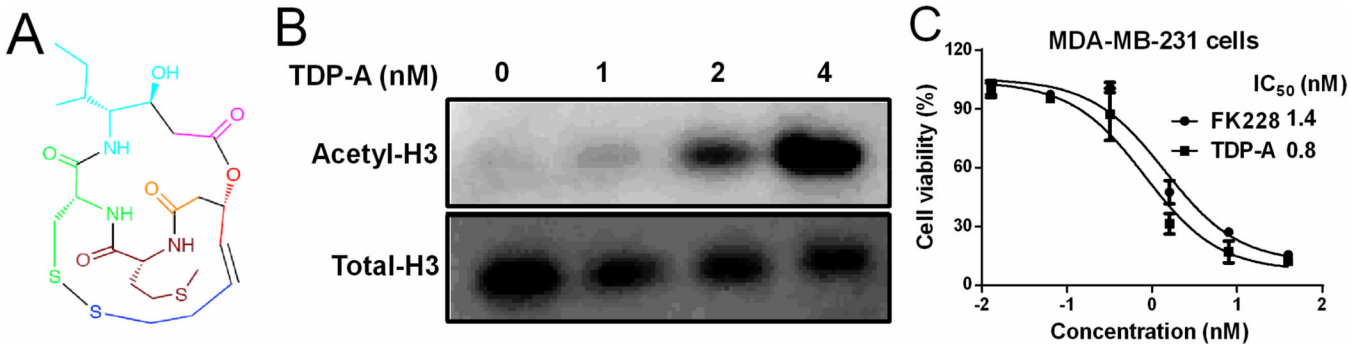

Figure 1. TDP-A inhibited breast cancer cell proliferation at nanomolar concentrations

(A) Chemical structure of TDP-A with building blocks coded in colors. (B) Representative western blot for H3 expression (acetylated and total) in MDA-MB-231 breast cancer cells after 24 h of treatment with TDP-A at the concentrations up to 4 nM. (C) The *in vitro* cytotoxicity of TDP-A against MDA-MB-231 cells after 72 h incubation, measured by MTS assay.

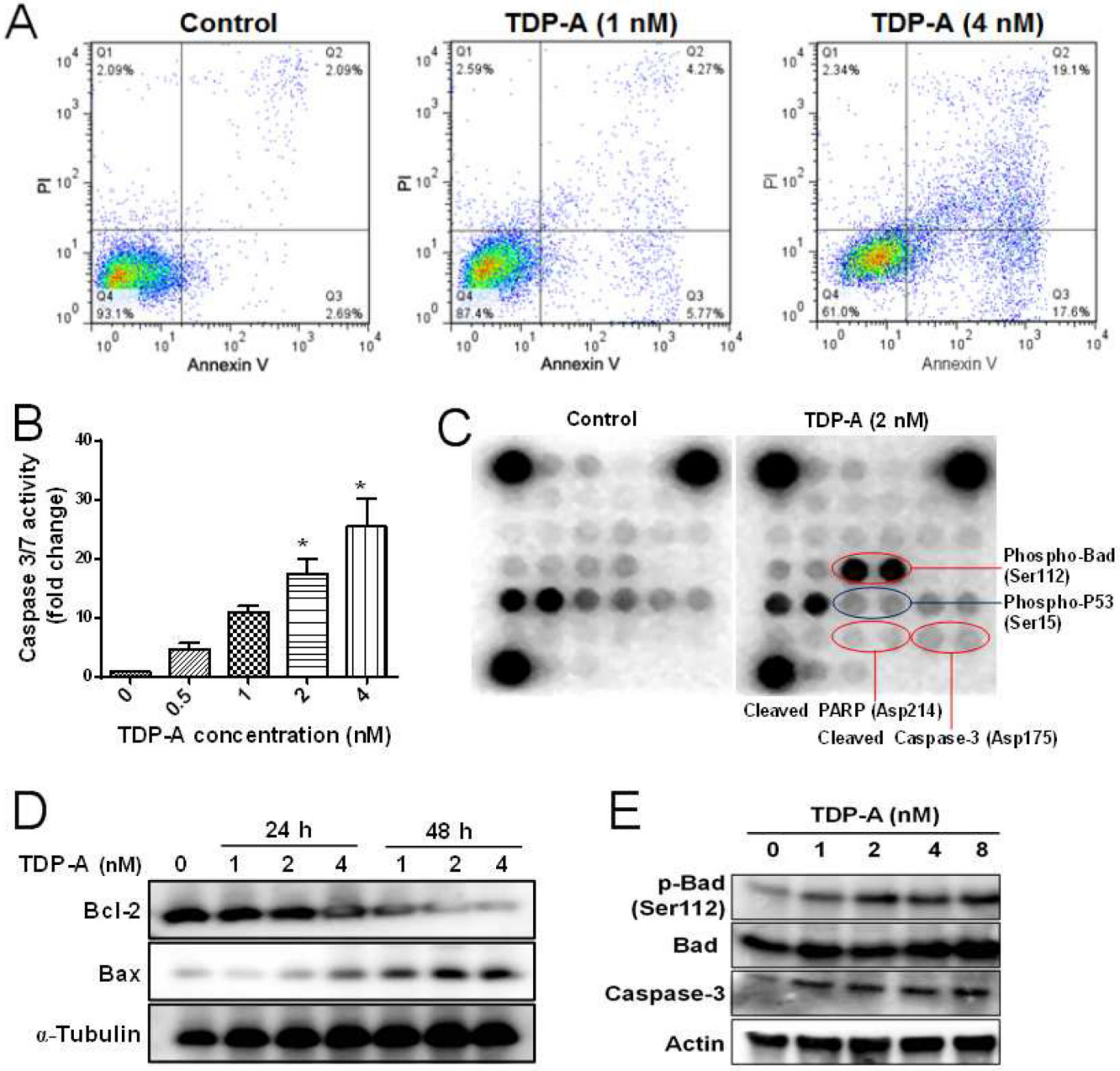

Figure 2. TDP-A induced apoptosis in MDA-MB-231 breast cancer cells

(A) Flow cytometric analysis of apoptosis by annexin V/PI dual staining assay after TDP-A treatment (1 and 4 nM) for 48 h. (B) The activities of caspase 3/7 in MDA-MB-231 cells after treatment with various concentrations of TDP-A (0, 0.5, 1, 2 and 4 nM) for 24 h. (C) Chemiluminescent array images of the PathScan Intracellular Signaling array kit in MDA-MB-231 cells treated with TDP-A (2 nM) for 24 h. (D) Western blot of Bcl-2 and Bax expression after TDP-A treatment for 24 h or 48 h. (E) Western blot of phosphor-Bad (Ser112), Bad, caspase-3 protein expression after TDP-A treatment (24 h).

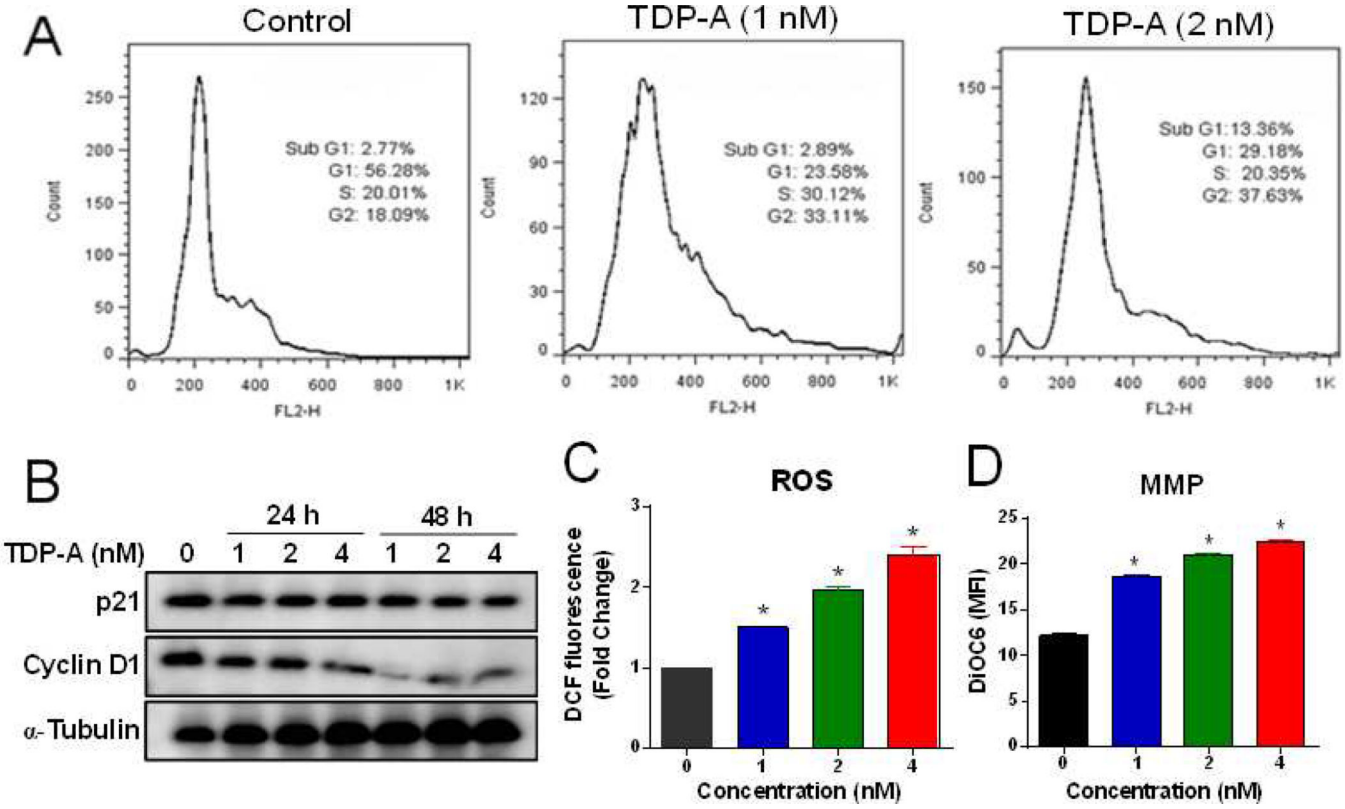

Figure 3. Effect of TDP-A on cell cycle progression, production of ROS and mitochondrial integrity in MDA-MB-231 cells

(A) Cells were treated with different concentrations of TDP-A for 24 h. The cell cycle analysis was conducted by FACScan flow cytometry. (B) Western blot analysis of p21 and cyclin D1 expression after TDP-A treatment for 24 h or 48 h. (C) TDP-A induced the production of ROS in MDA-MB-231 cells. Intracellular ROS was analyzed by flow cytometry after DCFDA probe staining. (D) TDP-A increased the mitochondrial membrane potential (MMP) as assayed by DiOC6 dye staining.

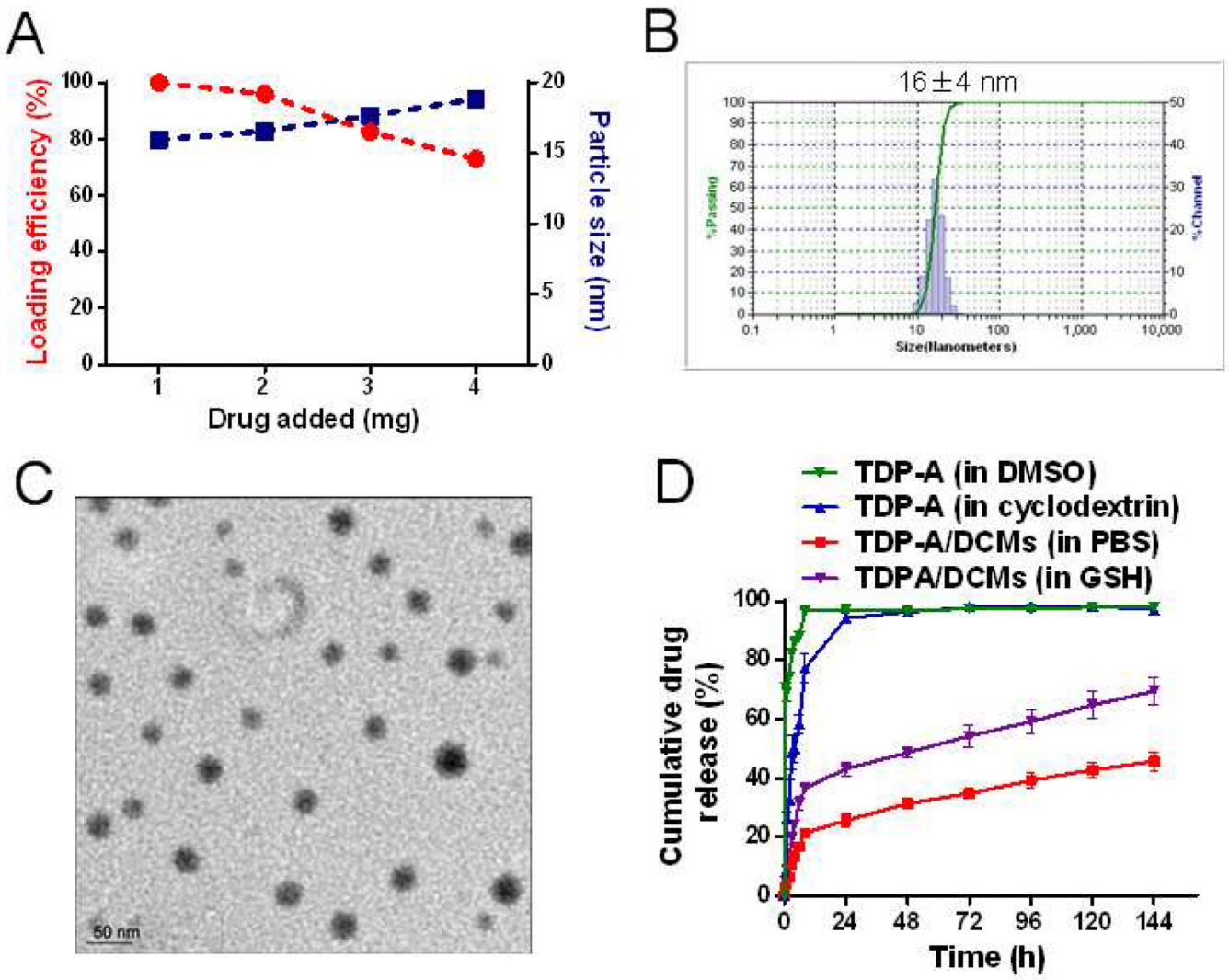

Figure 4.

(A) The loading efficiency and particle size of TDP-A/DCMs versus the amount of drug added at initial loading. The final concentration of the polymers was kept at 20 mg/mL. Representative DLS size distribution (B) and TEM image (C) of TDP-A/DCMs (TDP-A loading was 1 mg/mL; TEM scale bar: 50 nm). (D) Cumulative drug release profile of TDP-A/DCMs in PBS or GSH (10 mM) when compared to that of free TDP-A dissolved in cyclodextrin or DMSO. Values reported are the mean diameter ± SD for triplicate samples.

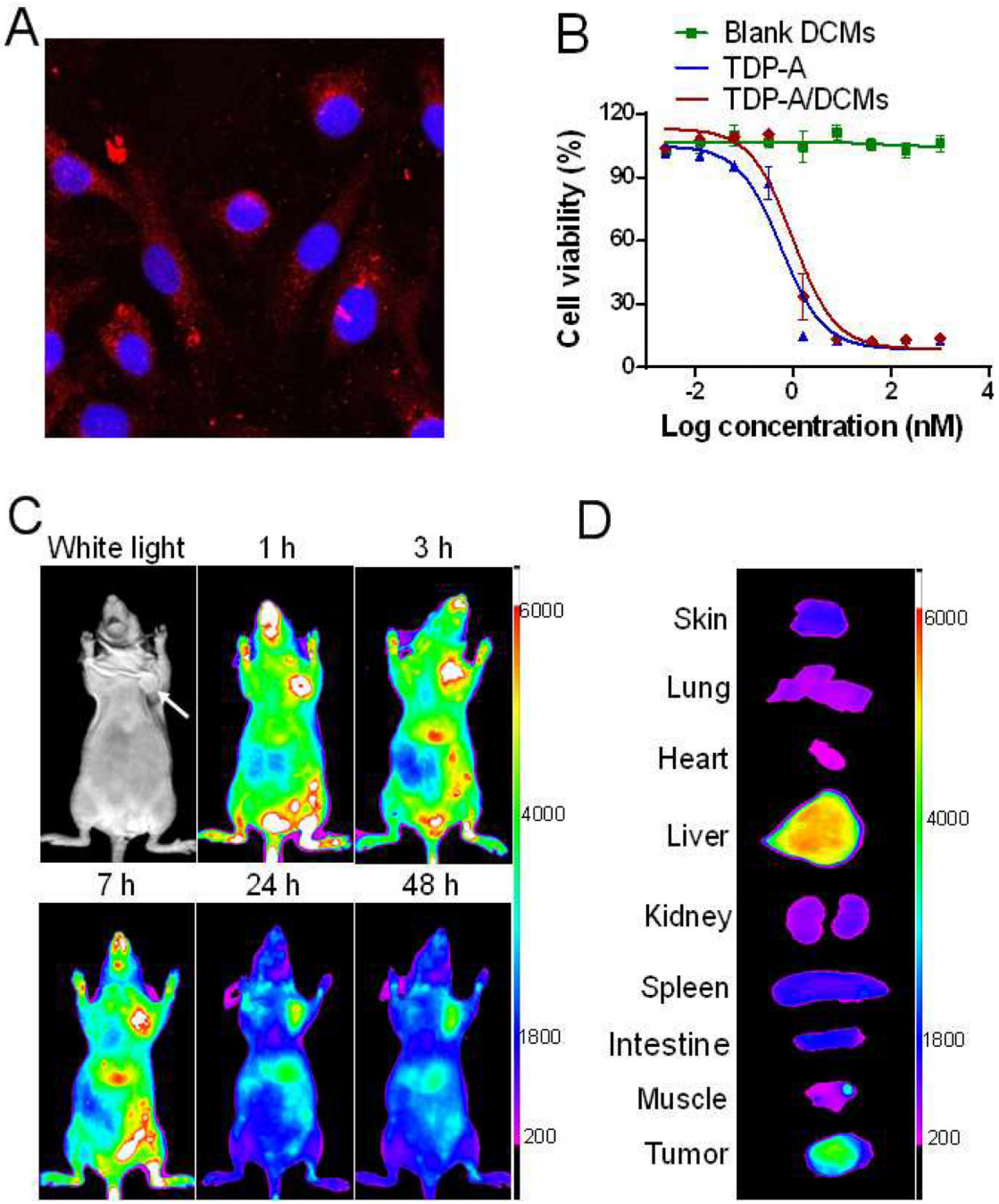

Figure 5.

(A) Confocal images showing the intracellular uptake of DiD fluorescently labeled DCMs in MDA-MB-231 cells after 4-h incubation. (B) The *in vitro* cytotoxicity of TDP-A/DCMs against MDA-MB-231 cells after 72 h incubation, measured by MTS assay. TDP-A loading in DCMs was 1 mg/mL. (C) *In vivo* NIRF optical images of orthotopic MDA-MB-231 tumor xenograft bearing mice after intravenous injection of DiD-TDP-A/DCMs. (D) *Ex vivo* NIRF image of dissected organs and tumor obtained at 48 h post-injection.

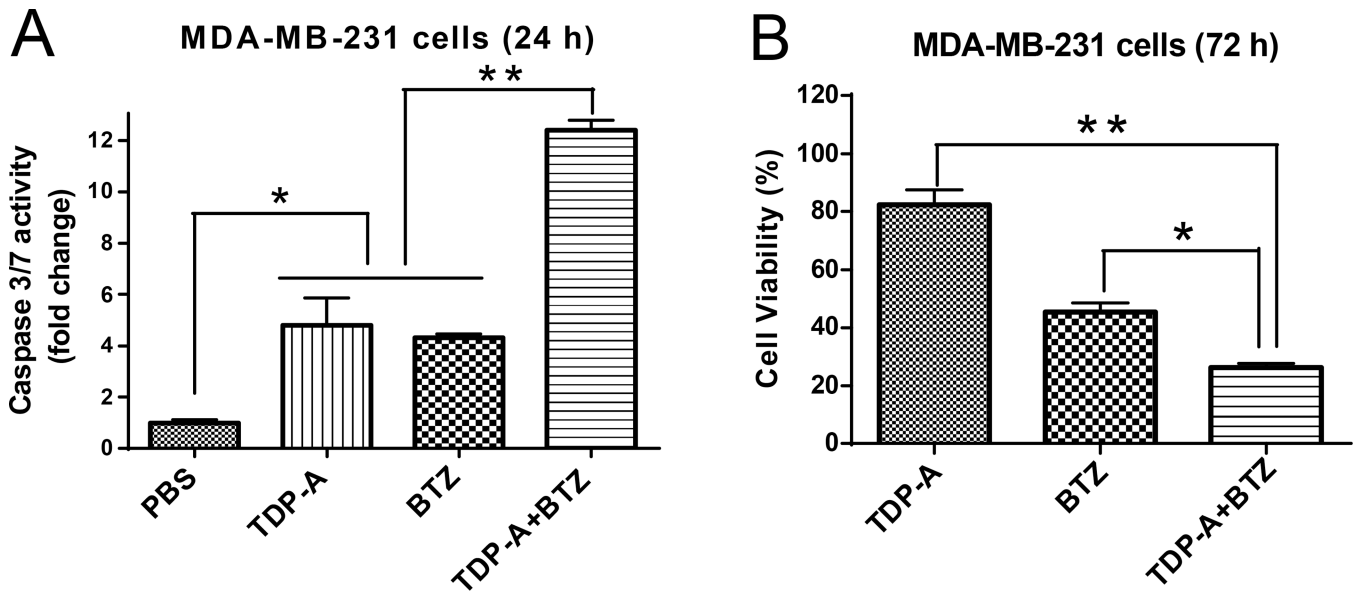

Figure 6.

Combination of TDP-A with BTZ induced synergistic apoptosis and cytotoxicity in MDA-MB-231 cells. The caspase 3/7 activity (A) and cell viability (B) of MDA-MB-231 cells treated with TDP-A (0.4 nM), BTZ (10 nM), and combined TDP-A with BTZ for the period of time as indicated in each panel.

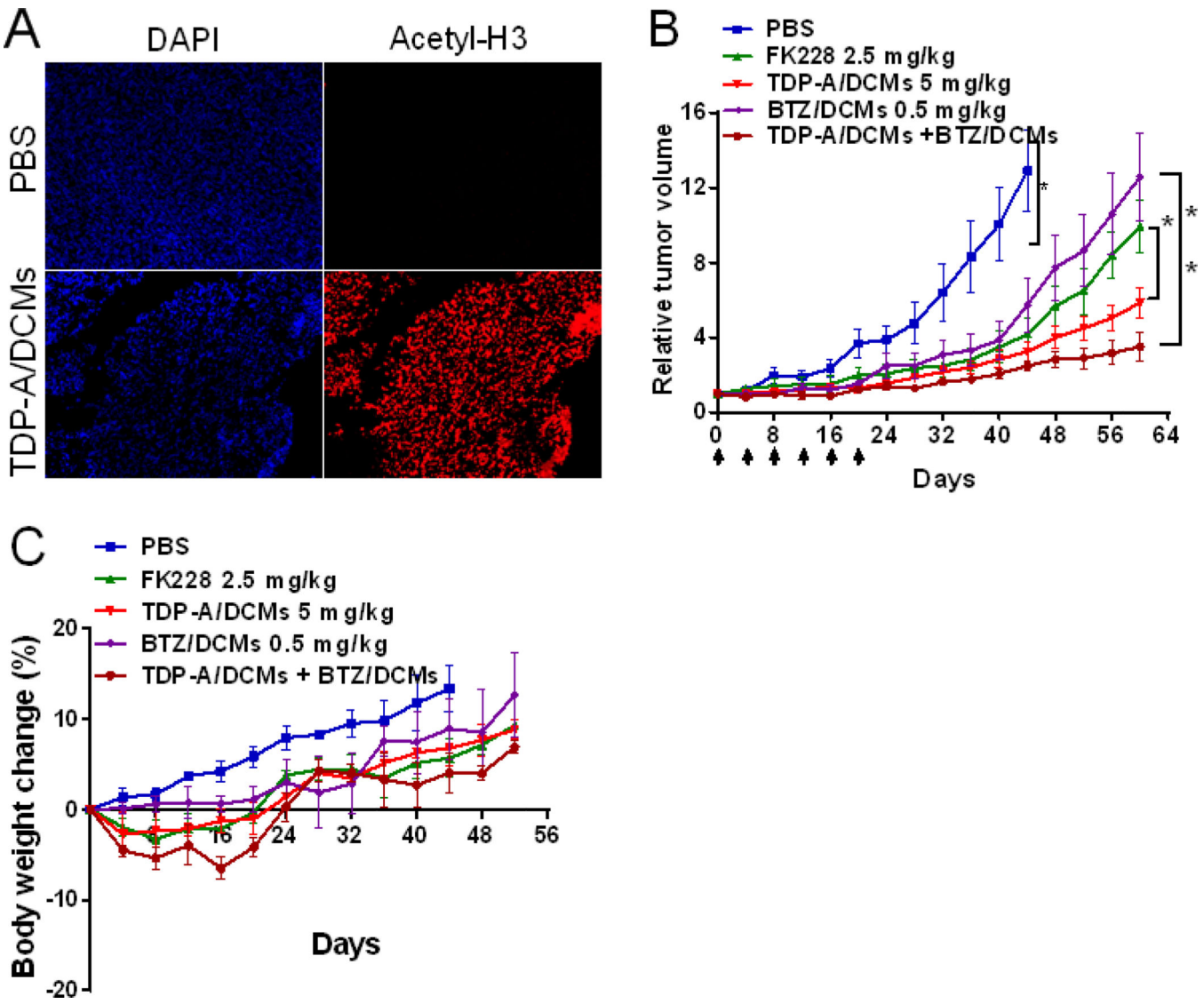

Figure 7.

(A) *In vivo* acetylated H3 expression in the MDA-MB-231 tumor xenograft at 24 h after the single dose of TDP-A/DCMs (5 mg/kg). *In vivo* tumor growth inhibition (B) and body weight changes (C) of orthotopic MDA-MB-231 tumor bearing mice treated with the micellar nanoformulations of TDP-A and BTZ. Tumor bearing mice were administered intravenously with PBS (control), free FK228 (2.5 mg/kg), TDP-A/DCMs (5 mg/kg), BTZ/DCMs (0.5 mg/kg), and TDP-A/DCMs (5 mg/kg) in combination with BTZ/DCMs (0.5 mg/kg), respectively. The loading of TDP-A and BTZ in DCMs were both 1 mg/mL. A total of six dosages were given every four days on day 0, 4, 8, 12, 16 and 20. Data represent mean ± SEM (n = 6–7).